Low-Frequency Sonophoresis: Ultrastructural Basis for Stratum Corneum Permeability Assessed Using Quantum Dots

Sumit Paliwal[1], Gopinathan K. Menon[2] and Samir Mitragotri[1]

Low-frequency sonophoresis (LFS) has been well documented to enhance the permeability of skin to macromolecular drugs via induction of localized transport regions. However, the organizational details of epidermis, specifically stratum corneum (SC), during sonophoresis are beyond the resolution limit of common histo-optical microscopy tools, which fail to reveal any notable structural alterations in these regions at a submicroscopic scale. Here we report, using quantum dots (QDs) as a tracer and confocal microscopy and transmission electron microscopy (TEM) (with OsO_4 and RuO_4 post-fixation) as visualization methods, on LFS-induced permeation pathways in the SC. QDs (20 nm diameter) penetrated well beyond the SC. TEM revealed that ultrasound significantly increased the frequency of occurrence of the otherwise scattered and separated lacunar spaces in the SC. A significant increase in lacunar dimensions was observed when 1% w/v sodium lauryl sulfate was added to the coupling medium. These studies show that LFS induces dilatation and higher connectivity of voids in the SC, possibly leading to formation of a three-dimensional porous network, which is capable of transporting QDs as well as macromolecules across the SC. This contention is consistent with previously conceived theoretical mechanistic understanding of LFS-induced enhanced transport across the skin.

INTRODUCTION

The stratum corneum (SC), the uppermost layer of the epidermis, offers a formidable barrier to permeation of molecules, except low molecular weight (<500 Da) and highly lipophilic molecules, that too in small doses (Mitragotri, 2004). This unusually high resistance of the SC arises from its robust brick (corneocytes) and mortar (intercellular lipid bilayers)-like structural organization. Tightly packed stacks of multiple lipid lamellae in the extracellular domains provide a highly tortuous and poorly permeable pathway, making it extremely difficult for molecules to diffuse across the skin (Elias, 1983).

Various mechanical, electrical, and chemical approaches have been used in the past to breach the SC barrier. While chemical penetration enhancers (Williams and Barry, 2004) interact directly with lipid bilayers, extracting and/or fluidiz-ing lipids in the SC, many physical methods such as jet injectors (Inoue et al., 1996) and microneedles (McAllister et al., 2003) employ mechanical perturbation of the SC for injecting molecules of interest into the skin. Electrical methods such as iontophoresis (Meyer et al., 1988) employ voltage gradients for solute migration or electroporation (Prausnitz et al., 1993), which involves high-voltage pulses for shorter time periods to open up pathways in the SC. Acoustical methods, including photoacoustic waves (Lee et al., 1998) and low-frequency ultrasound (Mitragotri et al., 1995), utilize mechanical waves to enhance SC permeability.

Ultrasound, particularly at low frequencies (20–100 kHz), has been shown to greatly enhance the permeability of skin, a phenomenon termed as sonophoresis. The efficacy of low-frequency sonophoresis (LFS) in delivering large-molecular-weight substances, for example, insulin through the skin, has been shown through both in vitro and in vivo studies (Mitragotri et al., 1995). It is now accepted that the basic principle behind LFS is inertial cavitation (violent growth and collapse of oscillating bubbles) in the coupling medium, which remains in contact with the skin. Acoustic spectral analysis and theoretical studies have suggested that the shock waves produced by symmetrical bubble collapse and the high-velocity microjets produced by asymmetrical bubble collapse are the primary sources for disruption of SC by LFS (Tezel and Mitragotri, 2003a).

Although the role of cavitation in LFS has been confirmed, the effect of cavitation on barrier structures of SC is largely

[1]Department of Chemical Engineering, University of California, Santa Barbara, California, USA and [2]California Academy of Sciences, Golden Gate Park, San Francisco, California, USA

Correspondence: Dr Samir Mitragotri, Department of Chemical Engineering, University of California, Santa Barbara, California 93106, USA. E-mail: samir@engineering.ucsb.edu

unknown. Unipolar photomechanical waves, which lack the tensile component (Perrie, 1973), have been shown to facilitate the delivery of molecules into the skin through lacunar dilatation (Menon et al., 2003). Photomechanical waves have been shown to expand the existing lacunar spaces (imperfections present in the lipid bilayer regions due to desmosomal breakdown involved in the natural desquamation process (Haftek et al., 1998)) to an extent that is believed to lead to a three-dimensional porous network for enhanced solute transport across the SC. A similar hypothesis has been proposed for LFS, but no experimental evidence has been reported (Tezel and Mitragotri, 2003b; Tezel et al., 2003). Mathematical models based on porous pathway model have been proposed to describe the transport properties during LFS (Tezel et al., 2002a, 2003), but lacked experimental validation for the existence of pores. Moreover, the question of how these LFS-induced SC modifications would manifest themselves at different length scales (centimeters to nanometers) has not been addressed earlier. In the context of presenting the basis for LFS-assisted macromolecular transport, the aim of the current study is to assess and provide a holistic picture of SC modifications during LFS, with an emphasis on the ultrastructural changes. This study also investigates the structural effects of LFS on skin with and without 1% w/v sodium-lauryl-sulfate (SLS) in the ultrasound coupling medium. Quantum dots (QDs) were mixed in the coupling medium and used as a tracer to delineate the permeation path within the SC. As QDs can be visualized both by fluorescence microscopy as well as transmission electron microscopy (TEM), we hoped to collect information at various length scales using the same tracer.

RESULTS

Histology and confocal laser-scanning microscopy

QDs were used as tracers since they can be visualized in fluorescence microscopy as well as TEM (Nisman et al., 2004). Penetration of QDs in the sonicated skin was highly heterogeneous at all length scales studied. At a macroscopic scale (millimeters), QDs were distributed in patches 1 mm in diameter, termed as localized transport regions (LTRs) (sulforhodamine B-penetrated skin surface, Figure 1a) (Tezel et al., 2002b), which occupied about 5% of exposed skin area under the conditions used in this study. Effect of ultrasound on skin structure and QD penetration was further assessed in LTR as well as non-LTR regions using confocal microscopy (Figure 1b) and TEM (Figure 1c).

Histological studies using hematoxylin and eosin staining showed no structural changes at the microscopic level in the skin in both LTR and non-LTR regions (Figure 2b and c). These results, which are in agreement with previous studies (Mitragotri et al., 1996; Tezel and Mitragotri, 2003a; Tezel et al., 2004, 2005), confirmed that the effects of ultrasound on skin structure exist at the submicroscopic level. Further details on SC microstructure and QD penetration were obtained using confocal microscopy. In the non-LTR regions, QDs were restricted to the top layers of the SC (solid arrow, Figure 3a). Significant penetration of QDs was observed in the LTR regions (Figure 3b–d). However, penetration of QDs
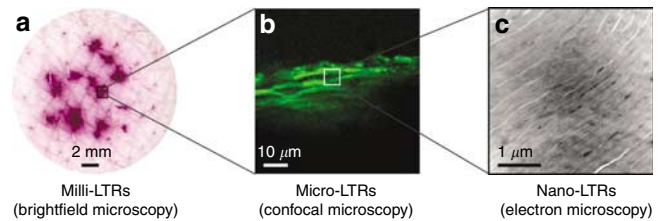

Figure 1. **Highly heterogeneous manifestation of low-frequency ultrasound-induced LTRs in the skin at different lengthscales.** (**a**) Macroscopic brightfield scan of skin surface showing patches of milli-LTRs imbibed with a colorimetric dye, sulforhodamine B. (**b**) Confocal micrograph of micro-LTRs showing preferential penetration of QDs within milli-LTRs. (**c**) At a nanoscale, the transmission electron micrograph shows the existence of nano-LTR pockets of QD penetration in the SC.
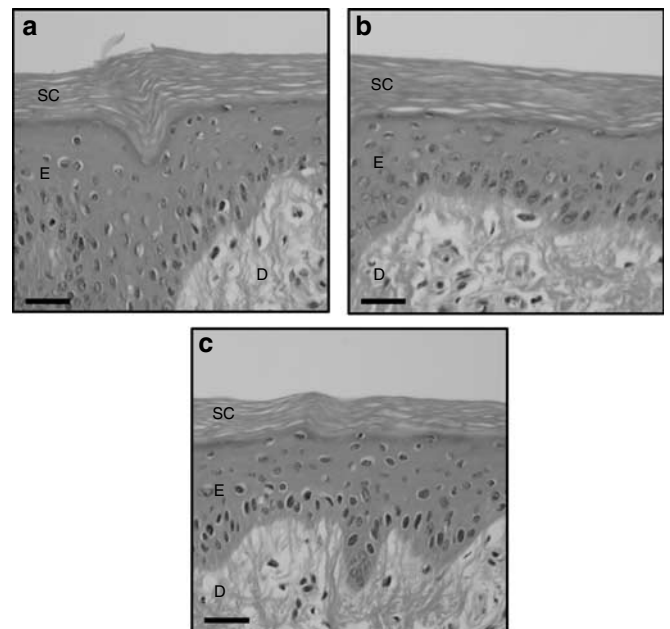

Figure 2. **Histology of skin upon LFS.** (**a**) H&E-stained cross-sectional view of a control skin sample. (**b**) H&E-stained cross-sectional view of a non-LTR region. (**c**) H&E-stained cross-sectional view of an LTR. No structural alterations were observed at light microscopic level between both LTR and non-LTR regions, and sonicated and control skin samples. SC: stratum corneum, E: epidermis, D: dermis. (**a–c**) Bar = 10 μm.

was heterogeneous even within the LTRs on a micrometer-length scale. Regions within LTRs that exhibited QD penetration ranged in widths of 40–80 μm with clear separation by regions with relatively little penetration (high-lighted boxed regions in Figure 3b and c). Heterogeneity of QD penetration was also evident in the direction normal to the SC surface. Layers of fluorescence were observed within the SC, which extended gradually to a diffused signal in the epidermis (Figure 3d). Penetration of QDs as deep as upto 60 μm was seen in the epidermis of the LTR regions.

Transmission electron microscopy
TEM studies were performed to further assess penetration of QDs at the nanometer length scale. Skin's ultrastructural
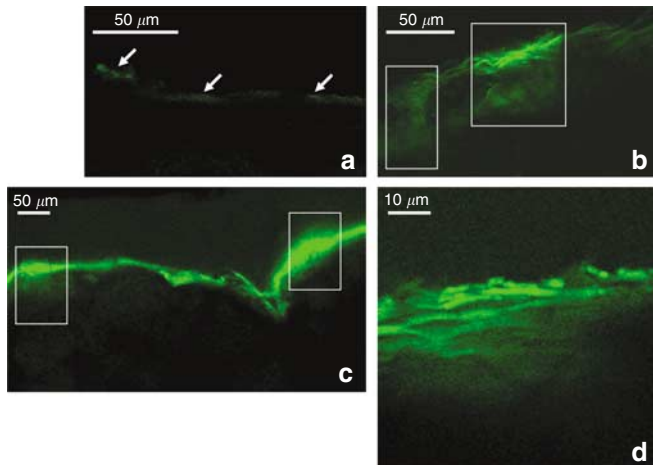
Figure 3. **Assessment of penetration of QDs in the LFS (with SLS)-treated skin with confocal laser scanning microscopy.** (**a**) The cross-sectional view of porcine skin in the non-LTR region. Arrows show QDs restricted to the top layers of the SC. (**b–d**) The cross-sectional view of porcine skin in the LTR region. Highlighted regions in (**b, c**) show regions within LTRs that exhibited high QD penetration, which ranged from 40–80 μm in width and upto 60 μm depth into the epidermis. (**d**) An enlarged micrograph of one such micro-LTR region.
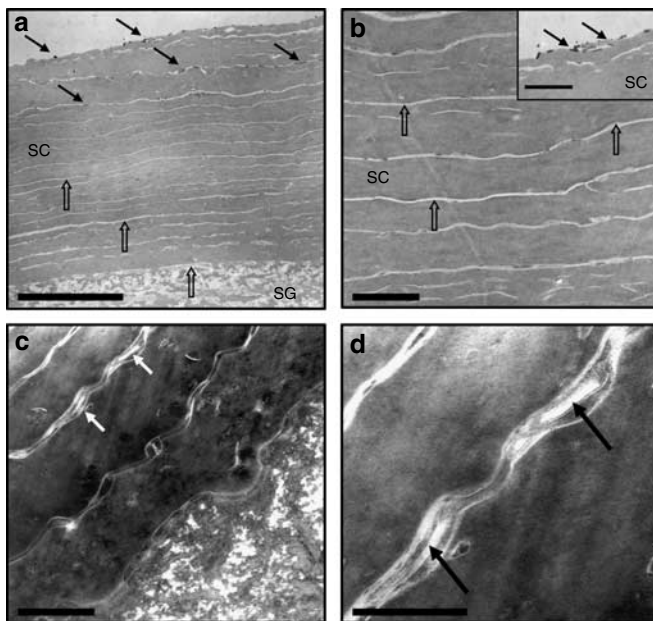

Figure 4. **Electron micrographs of SC and a part of stratum granulosum (SG) for control skin.** OsO_4 staining (**a**) at low and (**b**) at high magnification revealed the intact ultrastructure of the SC. Closed arrows show QDs trapped in superficial layers of the SC. Open arrows show extracellular domains of SC devoid of QD tracer. (**c**) RuO_4 staining at low and (**d**) high magnification show extracellular lipid lamellae and corneodesmosomes. Scattered and nonconnected lacunar domains are found within the intercellular lipid lamellae. Arrow in (**c**) and (**d**) show intercellular lacunar spaces in the SC. SC: stratum corneum, SG: stratum granulosum. (**a**) Bar = 5 μm, (**b**) Bar = 1 μm (inset: 1 μm), (**c**) Bar = 1 μm, and (**d**) Bar = 500 nm.

details were revealed by OsO_4 or RuO_4 post-fixation, with the former revealing cellular ultrastructural details and the latter specifically showing the structural organization of the barrier lipids. In the absence of ultrasound, QDs were found
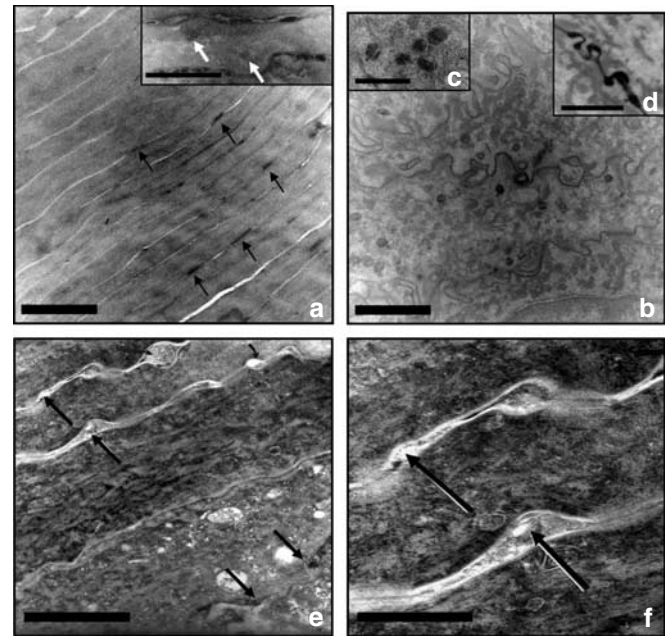

Figure 5. **Electron micrographs after application of ultrasound to porcine skin in the absence of SLS.** (**a**) Arrow in OsO_4-stained micrograph shows that QDs are uniformly distributed in localized pockets of the extracellular domains of the SC. Inset to the figure shows penetration of QDs in corneocytes. (**b**) TEM images confirmed the presence of QDs within intercellular spaces of the SG (viable epidermis) seen as an electron-dense region in the image. Insets (**c, d**) show a higher magnification image of QD saturated unsecreted lamellar bodies and intercellular spaces in the upper SG, respectively. RuO_4 staining (**e**) at low and (**f**) at high magnification, revealed lacunar dilatation (shown by arrow) and an increase in the frequency of occurrence of lacunar domains in the SC. (**a, b, e**) Bar = 1 μm and (**c, d, f**) Bar = 500 nm.

to be restricted to the top layers of SC (solid arrows, Figure 4a, inset in Figure 4b). SC in these samples exhibited the classical stacked corneocyte arrangement, packed around the lipid bilayers (open arrows, Figure 4a, enlarged view in Figure 4b). When stained by RuO_4, these samples showed the basic extracellular lamellar units comprising of a series of electron-dense and electron-lucent regions (Figure 4c, enlarged view in Figure 4d). Scattered, non-connected defects (lacunae) within the intercellular lipid lamellae were found in the controls (arrows, Figure 4c and d).

Application of ultrasound induced significant penetration of QDs within the lipid regions of SC (black arrows, Figure 5a). QDs were locally present at a few sites of corneodesmosomes and occasionally even inside the corneocytes (inset in Figure 5a). QDs also penetrated in the intercellular spaces at the stratum granulosum–SC interface, within the secreted contents of lamellar bodies (Inset (c), Figure 5b) as well as that of the nucleated layers in the epidermis (inset (d), dark wavy lines in Figure 5b). RuO_4 staining indicated an increase in the frequency of lacunar spaces (arrows, Figure 5e; enlarged view in Figure 5f).

Application of ultrasound in the presence of SLS induced similar but more pronounced effects on QD penetration as well as basic SC ultrastructure. Pronounced expansion of the
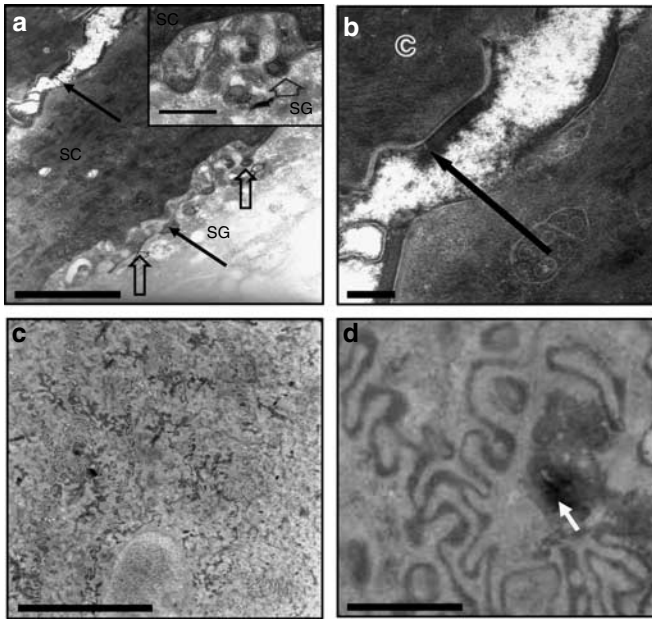
Figure 6. **Electron micrographs of RuO$_4$-stained porcine skin sections, after application of ultrasound in the presence of SLS.** (**a**) Large-scale lacunar domain expansion (closed arrow) was observed with a significant increase in their frequency of occurrence. At the SG–SC interface and the underlying SG cells, the secreted lamellar bodies' contents seemed to have been disrupted (open arrow) (inset shows the enlarged view of the SG–SC interface). (**b**) At high magnification, QDs were seen to be trapped in the intercellular regions in the SC. QD aggregation is shown as solid arrows in (**a**, **b**). (**c**) Pronounced penetration of QDs was observed in the epidermis. (**d**) QDs were localized primarily in the intercellular spaces in the epidermis (solid arrow).
C: corneocyte. (**a**) Bar = 500 nm (inset: 100 nm), (**b**) Bar = 50 nm, (**c**) Bar = 10 μm, and (**d**) Bar = 1 μm.
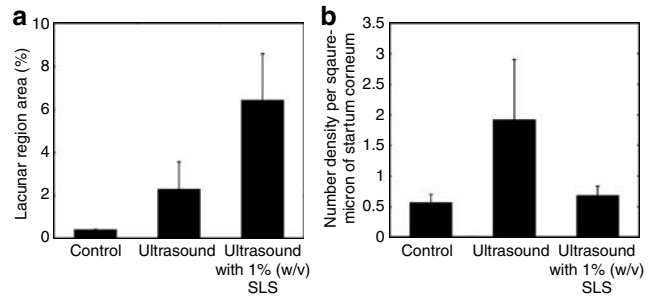

Figure 7. **Transmission electron micrographs of SC were processed by image analysis tools to identify and quantify lacunar regions present in control, ultrasound-treated, and ultrasound-SLS-treated skin.** (**a**) Area density of lacunar regions increased in ultrasound treated samples (Student's *t*-test: *P*<0.001) or ultrasound-SLS treatment compared to controls (Student's *t*-test: *P*<0.001) (single-factor ANOVA: *P*<0.001). (**b**) Number density of lacunar regions increased upon ultrasound exposure (Student's *t*-test: *P*=0.029), but was comparable to control for ultrasound-SLS treatment (Student's *t*-test: *P*=0.365).

SLS-treated samples. The mean lengths of lacunar regions were 183.9 ± 95.03, 240.2 ± 274.9, and 537.5 ± 422.9 nm in controls, ultrasound-treated, and ultrasound-SLS-treated samples, respectively. Mean widths of lacunar regions for the same populations were 48.1 ± 12.09, 70.4 ± 44.3, and 184.0 ± 144.9 nm, respectively.

DISCUSSION

The effects of LFS on skin are heterogeneous in nature. At a macroscopic level, the regions of interest for transdermal delivery are characterized by highly permeable spots, called LTRs, which have been reported previously. In the current study, both LTR and non-LTR regions were examined for QD penetration and structural changes.

QDs were chosen in these experiments due to several advantages that they provide as tracers. QDs are small enough to enter the SC during LFS, yet they are large enough to avoid diffusion in the SC. QDs are unique tracers in that they can be visualized by fluorescence microscopy as well as TEM. QDs' high electron density makes them good tracers in TEM studies (Nisman *et al.*, 2004); while wide excitation spectrum, high photostability, and minimal interference from tissue auto-fluorescence make them superior fluorophores for fluorescence imaging. LFS delivered QDs deep into the skin, crossing the SC. One of the important conclusions of these studies is that the penetration of tracers in the presence of ultrasound is highly heterogeneous (Figure 1). At a macroscopic scale, the heterogeneity manifests as milli-LTRs on a length scale of 1 mm. At a microscopic scale, it manifests as micro-LTRs, the regions showing preferential penetration of QDs within milli-LTRs into regions spanning about 40–80 μm microns in width and upto 60 μm in depth. Even at a nanoscale, the images show the existence of nano-LTRs, upto 100 nm wide, and 300 nm long pockets of QD penetration. At this length scale, QDs were distributed within the intercellular lipids, corneodesmosome junctions, and occasionally into corneocytes. Presence of SLS significantly promoted the penetration of QDs both in the SC and epidermis.

lacunar spaces (Figure 6a, enlarged view in Figure 6b), with QDs localized in them (solid arrows, Figure 6a and b), was distinctively observed. Penetration of QDs was also evident within the intercellular spaces of the nucleated layers of epidermis. (Figure 6c, enlarged view in Figure 6d). Ultrasound-induced disruption is evident within the secreted lamellar body contents at the SC–stratum granulosum interface and even in the subjacent stratum granulosum cells (open arrows, inset and Figure 6a). The skin samples shown in Figure 6 possessed a post-sonication electrical conductance of about 50-fold higher than the control sample.

Consistent with the visual observations, percentage lacunar area density in SC increased from $0.44 \pm 0.11\%$ in controls to $2.43 \pm 1.11\%$ in ultrasound-exposed and $6.25 \pm 1.61\%$ in ultrasound-SLS-exposed SC samples (Figure 7a). The lacunae number density of SC was $0.62 \pm 0.18 \, \mu\text{m}^{-2}$ for control, $1.98 \pm 1.01 \, \mu\text{m}^{-2}$ for sonicated SC, and $0.76 \pm 0.21 \, \mu\text{m}^{-2}$ for ultrasound with SLS (Figure 7b). It is interesting that lacunar area density increased (*P*<0.001), but number density did not change for ultrasound-SLS treatment compared to controls (*P*=0.365). This reflects increased length and connectivity of lacunar regions in ultrasound-SLS-treated samples. Large lacunar regions (>1 μm in length and 500 nm in width), which were not observed in controls and ultrasound-treated samples, were observed in ultrasound-

Penetration of QDs was generally consistent with structural changes observed in electron microscopy. Histology showed no changes in SC and epidermis structure (Figure 2), thus attesting that the structural changes occur at a submicroscopic scale. TEM images with the help of OsO_4 or RuO_4 staining revealed that LFS induced ultrastructural changes only in the LTR region of the SC. The modifications were even more pronounced and propagated deeper up to the stratum granulosum layer when SLS was used in the coupling medium. SLS is a small anionic surfactant (288.4 Da) that can alter SC's intercellular domain by various methods, including lipid extraction, disruption of the lipid sheets, and denaturation of proteins (Elias, 1996; Fartasch *et al.*, 1998; Welzel *et al.*, 1998). TEM images showed that LFS caused the otherwise scattered and separated lacunar spaces in the porcine skin to expand and also increase in frequency of occurrence. Lacunar spaces represent domains embedded within the lipid bilayers and often relate to sites of subjacent corneodesmosome degradation (Haftek *et al.*, 1998). Presence of lacunar spaces has been reported in electron-microscopy images of SC obtained using hydrophilic and hydrophobic tracers (Menon and Elias, 1997).

The electron micrographs suggest that lacunar imperfections, which manifest themselves as distinct closed regions in the normal SC, upon ultrasound exposure, may increase in number and yield higher connectivity to form a transient three-dimensional network, capable of transporting macromolecules. This hypothesis is consistent with lacunar-quantification studies revealing that exposure of ultrasound increases the number density of lacunar defects in the SC. The dimensions of lacunar regions formed by LFS are comparable to those in controls; however, LFS with SLS significantly changed the dimensions of lacunar regions, leading to increased connectivity. LFS along with SLS may expand lacunar spaces through two mechanisms. First, ultrasound can act on its own through its secondary effects, such as high-pressure shock waves and high-velocity microjets to submicroscopically disrupt the lipids and create more and wider lacunar imperfections in the SC interstices. Second, in the presence of SLS, LFS can deliver SLS to lipid bilayers and then, leaving SLS to result in extraction or phase separation of the bilayers, further enhance the lacunar dilatation and its occurrence frequency. SLS, at high concentrations and long contact times, is known to produce large-scale phase separations in the SC lipid bilayers and lacunar continuities (Menon *et al.*, 1998). However, in the absence of ultrasound, it is unlikely that significant amounts of SLS penetrate deep into the SC, given that a typical contact time of SLS with skin is a few minutes and the concentration in the coupling medium is 1% w/v. In the presence of ultrasound, however, significant quantities of SLS could penetrate into the SC. Thus, the effects observed in the presence of ultrasound and SLS represent their combined action.

It is not surprising that decrease in skin's barrier properties relates well with dilation in lacunar domains. Various other techniques to enhance transport across the skin, such as prolonged occlusion, chemical solvents (Menon *et al.*, 1998),

and photomechanical waves (Menon *et al.*, 2003), have reported lacunar distention. Certain skin disorders with compromised permeability barrier have also been found with the presence of blown-up lacunar ultrastructure. Fartasch (1997) reported formation of intercellular dilatations in psoriatic SC and concluded it to be the cause of altered epidermal barrier structure. Oleic acid-induced comedones in hairless mice with impaired water barrier function also showed incomplete lipid bilayer structure and prominent dilatation in lacunar domains (Choi *et al.*, 1997).

The proposed role of lacunar spaces in transport during LFS is consistent with the previous experimental and theoretical studies. Specifically, it has been proposed that LFS induces defects in lipids (Tezel *et al.*, 2002a, 2003) and this breach in the skin's barrier has been modeled as an opening of a wide distribution of pores in the SC, albeit not much physical evidence has been provided in these studies. In agreement with others (Menon *et al.*, 1994, 2003; Menon and Elias, 1997), our observations suggest that the extended lacunar spaces may symbolize LFS-induced permeation pathways in the SC.

Conclusions

The studies presented here describe the ultrastructural effects of low-frequency ultrasound on skin. It has been previously shown that the effects of ultrasound on skin are mediated through acoustic cavitation. Secondary effects of ultrasound due to oscillation and collapse of bubbles are implied in the observed ultrastructural effects. The effects of ultarsound on skin structure are submicroscopic in nature. No detectable destructive effect on the morphology of SC or epidermal cells could be found in histology. The effect of ultrasound is seen primarily on the intercellular lipids, as revealed by TEM. Quantification of TEM images showed that LFS increased the spatial frequency of occurrence of lacunae, which could possibly lead to an interconnecting three-dimensional network that increases solute transport.

MATERIALS AND METHODS
Application of ultrasound
Experiments were carried out with freshly excised full-thickness porcine skin (Yorkshire). Animals were killed using pentobarbital (100 mg/kg). Skin on the back and the lateral flank was harvested immediately after killing the animal. The underlying fat was removed and the skin was cut into small pieces ($2.5 \times 2.5 \, cm^2$). The procedures involving animal handling were approved by the institutional animal care and use committee of the University of California, Santa Barbara. Skin pieces with no visible imperfections such as scratches and abrasions were immediately mounted on a Franz diffusion cell (Permegear, Hellertown, PA). Only skin having an initial resistivity of $30 \, k\Omega \, cm^2$ or more was used to ensure that the skin was intact. The receiver compartment was filled with PBS (Sigma-Aldrich, St Louis, MO). The PBS solution was prepared using Milli-Q® water (Millipore, Billerica, MA) (18.2 MΩ resistance) and had a phosphate concentration of 0.01 M and NaCl concentration of 0.137 M. The donor compartment was filled with a solution of 2 mM colorimetric dye sulforhodamine B in PBS, and, depending on the experiment, also contained sodium lauryl sulfate (SLS) (1%

weight/volume). For tracing experiments, QDs (Cat. #1004-1, Quantum Dot Corp., Hayward, CA) were also added to the donor compartment at a final concentration of $2 \times 10^{-6} \, \mu M$. LFS is known to induce high-permeability spots on the skin, termed as LTRs (Tezel et al., 2001). Sulforhodamine B was added to the donor compartment to identify the location of LFS-induced LTRs. LTRs were identified by intense spots generated by penetration of sulforhodamine B. LTR and non-LTR regions were evaluated separately. Other confirmatory experiments were also performed with QDs alone in the donor compartment (without SLS and sulforhodamine B), so as to be able to distinguish QDs from the OsO_4 reactive components of SLS or the colorimetric dye, in electron microscopic examination.

A 600-W sonicator (Sonics & Materials, Newtown, CT) operating at a frequency of 20 kHz was used for ultrasound application. Before each experiment, the device was tuned using the procedure specified by the manufacturer. The ultrasound transducer was placed at a distance of 5 mm from the skin in the donor chamber. A 50% duty cycle was chosen (5 seconds on, 5 seconds off). This choice of duty cycle was made to minimize thermal effects and was otherwise arbitrary. The ultrasonic intensity was 2.4 W/cm^2, as measured by methods described in literature (Tezel et al., 2001). This value corresponds to a setting of 10% on the sonicator. In order to minimize the thermal effects, a thermocouple was placed in the donor chamber to ensure that the temperature rise was $\leqslant 5^{\circ}C$.

Prior studies have shown that skin impedance is an excellent indicator of skin permeability in the presence of ultrasound (Tezel et al., 2003). Skin conductivity (or conversely skin resistivity) was used as a measure of skin permeabilization. A 4-mm Ag/AgCl disk electrode (Invivo Metrics, Healdsburg, CA) was introduced in donor and receiver compartments for skin conductivity measurements during the experiment. A 100 mV rms AC signal (10 Hz) was applied across the electrodes (Agilent 33120A) and the current was recorded using a multimeter (Fluke). Detailed description of the resistivity measurement setup is reported in Tezel et al. (2001). In the presence of SLS, skin conductivity was increased to about 50-fold (corresponding to a sonication time of about 3 minutes) compared to the untreated skin.

Histology, TEM and confocal imaging

Following the treatment, skin tissues were fixed in 10% formalin overnight and embedded in paraffin. LTRs and non-LTRs were fixed separately. Tissue sections (5 μm thick) of these samples were stained with hematoxylin and eosin for histological examination. TEM was used for skin's ultrastructural analysis and QD penetration. Skin tissue samples, post-treatment, were immediately fixed in Karnovsky's fixative for 1 hour at room temperature and then overnight at 4$^{\circ}C$ in the same fixative. The samples were then washed in cacodylate buffer and post-fixed either in 1% OsO_4 or 0.5% RuO_4. Subsequently, the samples were dehydrated in graded series of ethanol, embedded in a low-viscosity epon–epoxy mixture and sectioned. Thin sections were double stained with uranyl acetate and lead citrate and examined under an electron microscope operating at 80 kV. For skin samples exposed to QDs alone (without SLS and sulforhodamine B), the tissue was embedded with and without OsO_4 post-fixation, and both stained and unstained sections were examined.

Penetration of QDs in the skin was also analyzed using laser-scanning confocal microscopy. Thin LTR and non-LTR regions (~ 1 mm section) were cut out from the treated skin tissue samples and laterally placed on a glass slide with coverslip covering the cross-section of the tissue. QDs in the tissue sample were excited by argon laser (488 nm) or UV (405 nm) and observed in the emission rage of 505–525 nm, using a confocal microscope (Olympus FluoView 500, mounted on Olympus IX81 inverted microscope). Three skin samples for each condition were analyzed by confocal microscopy and TEM, respectively. Each sample yielded at least three LTRs and non-LTRs, which were then further sectioned into two or three parts (depending on the sample size) for confocal microscopy and TEM studies.

Lacunar region quantification

At least eight randomly selected TEM images of control, ultrasound-exposed, and ultrasound-SLS-exposed SC were quantified for lacunar regions using image analysis tools (ImageJ, National Institutes of Health). Images were processed by taking fast Fourier transform and/or by convolving images, followed by thresholding to extract lacunar regions from the images. The processed images thus obtained only represented lacunar regions, which were then quantified by the ''Analyze Particle'' tool of ImageJ software. Lacunar area density, number density, and size distribution were quantified for control, ultrasound-exposed, and ultrasound-SLS-exposed skin samples.

Statistical analysis

To test the significance of lacunar region properties upon ultrasound treatment, analysis of variance (ANOVA) and Student's t-test (two-tailed, heteroscedastic test) were applied to the data set.

REFERENCES

Choi EH, Ahn SK, Lee SH (1997) The changes of stratum corneum interstices and calcium distribution of follicular epithelium of experimentally induced comedones (EIC) by oleic acid. Exp Dermatol 6:29–35

Elias PM (1983) Epidermal lipids, barrier function, and desquamation. J Invest Dermatol 80(Suppl):44s–9s

Elias PM (1996) The stratum corneum revisited. J Dermatol 23:756–8

Fartasch M (1997) Epidermal barrier in disorders of the skin. Microsc Res Tech 38:361–72

Fartasch M, Schnetz E, Diepgen TL (1998) Characterization of detergent-induced barrier alterations – effect of barrier cream on irritation. J Investig Dermatol Symp Proc 3:121–7

Haftek M, Teillon MH, Schmitt D (1998) Stratum corneum, corneodesmosomes and ex vivo percutaneous penetration. Microsc Res Tech 43:242–9

Inoue N, Kobayashi D, Kimura M, Toyama M, Sugawara I, Itoyama S et al. (1996) Fundamental investigation of a novel drug delivery system, a transdermal delivery system with jet injection. Int J Pharm 137:75–84

Lee S, McAuliffe DJ, Flotte TJ, Kollias N, Doukas AG (1998) Photomechanical transcutaneous delivery of macromolecules. J Invest Dermatol 111:925–9

McAllister DV, Wang PM, Davis SP, Park JH, Canatella PJ, Allen MG et al. (2003) Microfabricated needles for transdermal delivery of macromole-

cules and nanoparticles: fabrication methods and transport studies. *Proc Natl Acad Sci USA* 100:13755–60

Menon GK, Bommannan DB, Elias PM (1994) High-frequency sonophoresis: permeation pathways and structural basis for enhanced permeability. *Skin Pharmacol* 7:130–9

Menon GK, Elias PM (1997) Morphologic basis for a pore-pathway in mammalian stratum corneum. *Skin Pharmacol* 10:235–46

Menon GK, Kollias N, Doukas AG (2003) Ultrastructural evidence of stratum corneum permeabilization induced by photomechanical waves. *J Invest Dermatol* 121:104–9

Menon GK, Lee SH, Roberts MS (1998) Ultrastructural effects of some solvents and vehicles on the stratum corneum and other skin components: evidence for an extended mosaic-partitioning model of the skin barrier. In: *Dermal Absorption and Toxicity Assessment.* (Roberts MS and Walters KA, eds), New York: Marcel-Dekker, Inc., 727–51

Meyer BR, Kreis W, Eschbach J, O'Mara V, Rosen S, Sibalis D (1988) Successful transdermal administration of therapeutic doses of a polypeptide to normal human volunteers. *Clin Pharmacol Ther* 44:607–12

Mitragotri S (2004) Breaking the skin barrier. *Adv Drug Deliv Rev* 56:555–6

Mitragotri S, Blankschtein D, Langer R (1995) Ultrasound-mediated transdermal protein delivery. *Science* 269:850–3

Mitragotri S, Blankschtein D, Langer R (1996) Transdermal drug delivery using low-frequency sonophoresis. *Pharm Res* 13:411–20

Nisman R, Dellaire G, Ren Y, Li R, Bazett-Jones DP (2004) Application of quantum dots as probes for correlative fluorescence, conventional, and energy-filtered transmission electron microscopy. *J Histochem Cytochem* 52:13–8

Perrie AN (1973) Theory of momentum transfer to a surface with a high-power laser. *Phys Fluids* 16:1435–40

Prausnitz MR, Lau BS, Milano CD, Conner S, Langer R, Weaver JC (1993) A quantitative study of electroporation showing a plateau in net molecular transport. *Biophys J* 65:414–22

Tezel A, Dokka S, Kelly S, Hardee GE, Mitragotri S (2004) Topical delivery of anti-sense oligonucleotides using low-frequency sonophoresis. *Pharm Res* 21:2219–25

Tezel A, Mitragotri S (2003a) Interactions of inertial cavitation bubbles with stratum corneum lipid bilayers during low-frequency sonophoresis. *Biophys J* 85:3502–12

Tezel A, Mitragotri S (2003b) On the origin of size-dependent tortuosity for permeation of hydrophilic solutes across the stratum corneum. *J Control Rel* 86:183–6

Tezel A, Paliwal S, Shen Z, Mitragotri S (2005) Low-frequency ultrasound as a transcutaneous immunization adjuvant. *Vaccine* 23:3800–7

Tezel A, Sens A, Mitragotri S (2003) Description of transdermal transport of hydrophilic solutes during low-frequency sonophoresis based on a modified porous pathway model. *J Pharm Sci* 92:381–93

Tezel A, Sens A, Mitragotri S (2002a) Incorporation of lipophilic pathways into the porous pathway model for describing skin permeabilization during low-frequency sonophoresis. *J Control Rel* 83:183–8

Tezel A, Sens A, Tuchscherer J, Mitragotri S (2001) Frequency dependence of sonophoresis. *Pharm Res* 18:1694–700

Tezel A, Sens A, Tuchscherer J, Mitragotri S (2002b) Synergistic effect of low-frequency ultrasound and surfactants on skin permeability. *J Pharm Sci* 91:91–100

Welzel J, Metker C, Wolff HH, Wilhelm KP (1998) SLS-irritated human skin shows no correlation between degree of proliferation and TEWL increase. *Arch Dermatol Res* 290:615–20

Williams AC, Barry BW (2004) Penetration enhancers. *Adv Drug Deliv Rev* 56:603–18